**Citation**: Chunju Wang, Xueyi Chen, Da Qian, et al. Research on deposition process of transition multilayer films for metal-based sensors. *Journal of Harbin Institute of Technology(New Series)*. DOI:10.11916/j.issn.1005-911.25058

# Research on Deposition Process of Transition Multilayer Films for Metal-Based Sensors

*Chunju Wang*, Xueyi Chen, Da Qian, Jinhui Xie, Haidong He*, Lining Sun and Yangjun Wang*

(*School of Mechanical and Electrical Engineering, Robotics and Microsystems Center, Soochow University, Suzhou 215131, China*)

**Abstract**: Metal-based Micro-Electro-Mechanical Systems (MEMS) thin film sensors can achieve accurate in-situ measurements and withstand harsh working conditions, large ranges, etc., with broad application prospects. However, there are significant differences in performance such as thermal matching between metallic substrates and functional films, which can easily lead to defects such as sensitive film detachment. For this reason, this paper carried out a study on the preparation process of Ti, Cr, and Ni transition layer films on stainless-steel substrates, and analyzed the influence of process parameters on the surface roughness and deposition rate of the films. Then, the influence of hybrid transition layers was studied from the viewpoint of the bonding force between the substrate and the insulation layer using the scratch tests. The results showed that the transition layer could significantly increase the bonding force between the $SiO_2$ insulation layer and the stainless-steel substrate, from 15 N to 45 N, indicating improved interfacial adhesion, which is beneficial for the reliability of metal-based MEMS sensors under harsh working conditions.

**Keywords**: metal-based MEMS sensor, multilayer films, surface roughness and deposition rate, bonding force, material performance matching

**CLC number**: TB31 **Document code**: A **Article ID**: 1005-9113(2026)00-0000-10

## 0 Introduction

Metal-Based MEMS (Micro-Electro-Mechanical Systems) sensors can be integrated with metallic structural components to achieve in-situ measurement, and own many advantages, such as high measurement accuracy, high integration, and good working-condition resistance. So, they have broad application prospects in multiple fields, such as dexterous robot hands[1-2], aero-engines and space vehicles[3-4], etc. A metal-based six-axis force/torque sensor for space robotic applications was developed using thin-film sputtering technology, in which Ti, SiC/$SiO_2$, and NiCr were employed as the transition layer, insulating layer, and functional layer, respectively[2]. With titanium alloy and nickel alloy as metallic substrates, the ZnO/titanium structure and NiCrAlY/$Al_2O_3$ were studied to fabricate temperature and strain sensors for health monitoring of an aero-engine, which operates under high-temperature conditions, and the thermal stability was analyzed by examining the microstructure evolution[5-7].

However, since the metallic substrate is a kind of excellent electrical conductor, insulating layer, such as $SiO_2$, $Al_2O_3$, etc., should be applied to isolate the electrical interconnection between the substrate and the sensitive functional layer of MEMS sensor[8]. The material compatibility between the metallic substrate and the insulating layer is very poor induced by different coefficients of thermal expansion. Some kinds of transition multilayer films are necessary to improve bonding performance for the metallic substrate of MEMS sensors[9]. González et al.[10] summarized the transition layer used in thin-film sensors for in-situ characterization of tool temperatures, and reference shows that Ti, Cr film is selected to promote adhesion of isolation layer, such as $SiO_2$, and $Al_2O_3$, etc. in metal-based sensors. To elucidate structure-property relationships, a Ti-Ni-Si

Recieve 2025-10-23.

Sponsored by the National Key Research and Development Program of China (Grant No.2022YFB4701000).

* Corresponding author: Chunju Wang, Ph.D, Professor. Email: cjwang@suda.edu.cn;
Haidong He, Ph.D, Associate Professor. Email: hdhe@suda.edu.cn.

thin-film system was prepared via combinatorial magnetron sputtering, and a corresponding thin-film phase diagram was constructed based on high-throughput X-ray diffraction characterization[10]. Feng and Zhang et al.[11-12] investigated the microstructural evolution of nitrogen-doped Ni/Ti multilayers, revealing that the grain size remained smaller than the individual layer thickness. In addition, interface roughness increased with increasing layer thickness in periodic multilayers, while nitrogen segregation at the interfaces effectively inhibited interlayer diffusion. The effects of Ar recoil particle energy on the interfacial characteristics and microstructure of Ni/Ti multilayers were examined by adjusting the sputtering pressure. The results showed that both interfacial width and roughness varied with decreasing sputtering pressure, accompanied by a transformation in the preferred orientation of Ni layers from a single (111) texture to a mixed (111)/(100) texture. These changes were attributed to the combined energetic effects of Ar recoil particles and the depositing Ni and Ti atoms[13]. Sakhonenkov et al.[14] conducted a systematic study on the chemical, structural, and magnetic properties of Ti/Ni multilayer systems and demonstrated that introducing ultrathin silicon buffer layers at the interfaces significantly suppressed intermetallic compound formation, likely due to the generation of titanium silicides. Reactive magnetron sputtering of Ni/Ti multilayers using Ar-$N_2$-$O_2$ gas mixtures further revealed that the incorporation of $N_2$ and $O_2$ reduced Ni grain size, resulting in smoother interfaces and suppressed interfacial roughness replication and interlayer diffusion[15]. Multilayer film architectures have also been explored to enhance the thermal stability and electrical conductivity of Pt-based nanocomposite films exposed to air at temperatures up to 1200 ℃. Among various adhesion layers, Ni, Zr, Y, and $CeO_x$ exhibited the highest stabilization temperatures[16]. Furthermore, by incorporating selected elements (Cr, Ni, and Si) into Zr-based multilayers, the stability and oxygen-barrier performance were systematically evaluated, with key influencing factors identified as grain boundary effects, oxygen diffusion coefficients, and Zr/X interdiffusion behavior[17]. To decrease the resistance of sputtered thin-film resistor grids and improve film adhesion, NiCr-based thin-film sensors deposited on 304 stainless steel substrates were annealed in a nitrogen atmosphere. The results indicated that annealing at 450 ℃ led to a reduction in resistance to approximately 1.77 kΩ, while the strongest film-substrate adhesion was achieved at 350 ℃ for 30 min, representing an improvement of about 37.5% compared with the as-deposited state. Enhanced adhesion reduced the likelihood of premature cracking or delamination, thereby extending the effective force measurement range[18]. Investigations shown above indicate that most of them were focused on the properties of functional films, for example, the insulating layer and the sensitive layer. Few studies have been carried out on transition multilayers.

This study investigates the deposition process of Ti, Cr, and Ni transition single layer using the stainless-steel substrate. And the surface roughness and deposition rate of the films are evaluated using AFM apparatus. Then, hybrid transition multilayers were deposited, and the influence on the bonding force between the substrate and the $SiO_2$ insulation layer was studied using scratch tests with different combinations of film materials and thicknesses. Also, the experimental results are compared with those without transition layers. The findings are analyzed from the viewpoint of bonding energy and atom mass.

## 1 Experimental Setup

### 1.1 Preparation for Stainless-Steel Substrate

The material of the metallic substrate is selected as the stainless-steel 17-4PH with high strength, hardness, corrosion resistance and small coefficient of thermal expansion. Its elements are shown in Table 1. The specimen is machined to the ø 20 mm×2 mm. Since the thickness of the film used in MEMS is very small, the thickness and surface roughness have an obvious effect on the bonding force and insulation performance between the transition and insulating layers. The stainless-steel substrate is carefully polished using mechanical polishing and electrochemical polishing, respectively. First, the specimen is mechanically polished by utilizing the automated machine MECATECH 300 SPS, and the parameters of mechanical polishing process are shown in Table 2. Then, the electropolishing process is applied using the polishing solution shown in Table 3, and the parameters shown in Table 4. The polished specimens are ultrasonically cleaned, and the surface roughness (*Ra*) is about 20 nm, which can meet the requirement of deposition process of multilayers for MEMS sensors.

**Table 1 Alloy elements of 17-4PH** $w(\%)$

| Cr | Ni | Cu | Nb | C | Si and Mn | Fe |
|---|---|---|---|---|---|---|
| 15.0–17.5 | 3.0–5.0 | 3.0–5.0 | 0.15–0.45 | ≤0.07 | ≤1.0 | Balance |

**Table 2 Parameters of mechanical polishing process**

| No. of process | Grit of sandpaper(grit) | Polishing cloth (μm) | Polishing solution | Time(min) | Force(N) | Turning speed |
|---|---|---|---|---|---|---|
| 1 | 600 | – | Water | 5 | 5 | 300 |
| 2 | 1200 | – | Water | 5 | 1 | 300 |
| 3 | 2000 | – | Water | 12 | 1 | 300 |
| 4 | 2400 | – | Water | 12 | 1 | 300 |
| 5 | – | 9 | 9 μm diamond suspension | 12 | 1 | 300 |
| 6 | – | 3 | 3 μm diamond suspension | 12 | 1 | 300 |
| 7 | – | 1 | 1 μm diamond suspension | 12 | 1 | 300 |

**Table 3 Polishing solution of electropolishing process**

| Component | Proportion(%) |
|---|---|
| phosphoric acid ($d$=1.70 g/cm$^3$) | 60 |
| sulfuric acid ($d$=1.84 g/cm$^3$) | 25 |
| Water | 15 |

Note: $d$ represents the density of the polishing solution.

**Table 4 Parameters of electropolishing process**

| Cathode | Cathode/Anode | Current(A) | Voltage(V) | Time(s) |
|---|---|---|---|---|
| 17-4PH | 2∶1 | 0.7 | 4.8 | 30 |

### 1.2 Deposition and Measurement Apparatus of Transition Layer

The transition layer films are deposited using a DC magnetron sputtering process with a deposition apparatus TRP-450 (produced by SKY Technology Development Co., Ltd. Chinese Academy of Sciences). During the deposition of thin films, there are mainly three parameters, such as working pressure of argon, bias voltage and sputtering time, which have an obvious effect on the quality of transition layers. In the investigation, their effects are analyzed in detail.

The surface roughness and thickness of deposited layers are evaluated by the atomic force microscope Dimension Icon AFM (produced by Bruker (Beijing) Scientific Technology Co. Ltd.).

The specimen with a deposited thin film is shown in Fig. 1 (a), and its surface roughness $Ra$ is measured using the Dimension Icon AFM. For each specimen, 9 square areas with a size of 5 μm×5 μm are selected to measure their surface roughness, as shown in Fig.1 (b), and the roughness of each area is measured 2 times. Then, a total of 18 data points is obtained, and the average value is calculated, which is used as the evaluation parameter. The thickness is measured at 5 intervals over 4 steps, as shown in Fig.1(b), and the average value is calculated using the total of 20 data points for every specimen. Also, the standard deviation value of these 20 data points is calculated to reflect the degree of dispersion of the film thickness dataset. The smaller the standard deviation value of the film thickness, the less the deviation from the average value, indicating a higher uniformity in film thickness. The thickness of the Ti thin film was measured, as shown in Fig. 2. The step height was measured six times, and the average value was taken as the film thickness.

### 1.3 Design of Transition Layer

Previous studies have shown that some elements, such as titanium, chromium and nickel etc., can increase the adhesion of coating films. To improve the bonding performance, a kind of transition layer with multilayers is designed to solve the material compatibility between the metallic substrate and insulating layers, as shown in Fig.3. The Ti layer is arranged adjacent to the metallic substrate; its thermal expansion characteristics and metal bonding capability are relatively well matched to those of the stainless-steel substrate, facilitating the formation of a stable initial interfacial bond. The Cr layer is positioned in the middle; its high interfacial bonding strength and low atomic diffusion activity play a key role in stress buffering and diffusion blocking. The Ni layer is located near the functional layer, and its thermal expansion behavior and surface chemical properties are more favorable for improving the deposition continuity and interfacial bonding quality of the heterogeneous interface. In addition, multilayer transition films can effectively reduce abrupt thermal strain at adjacent

interfaces by creating a gradient in the coefficient of thermal expansion, thereby exhibiting improved interfacial stability under high-temperature and thermal cycling conditions.

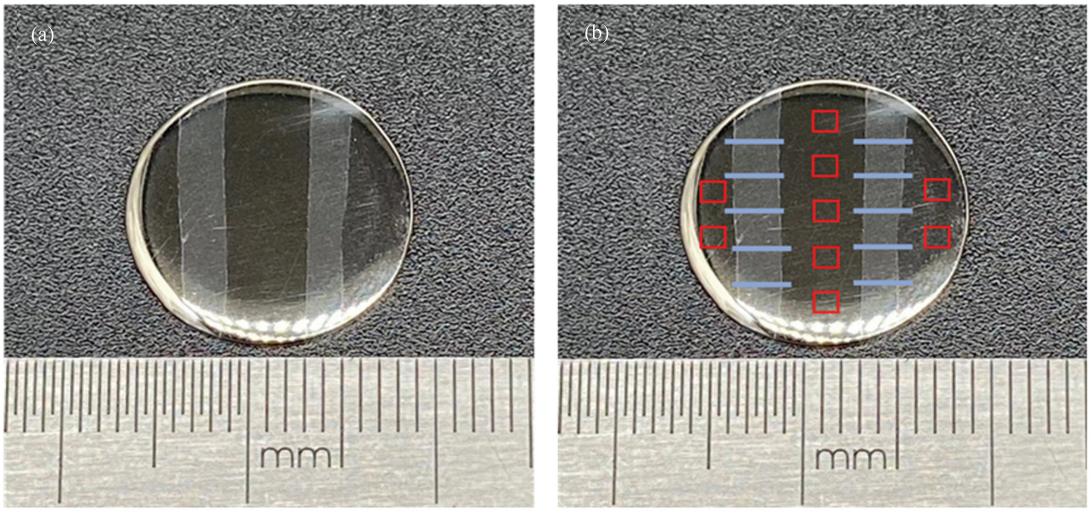


**Fig.1 (a) Specimen with thin film and (b) measurement points of surface roughness and thickness**

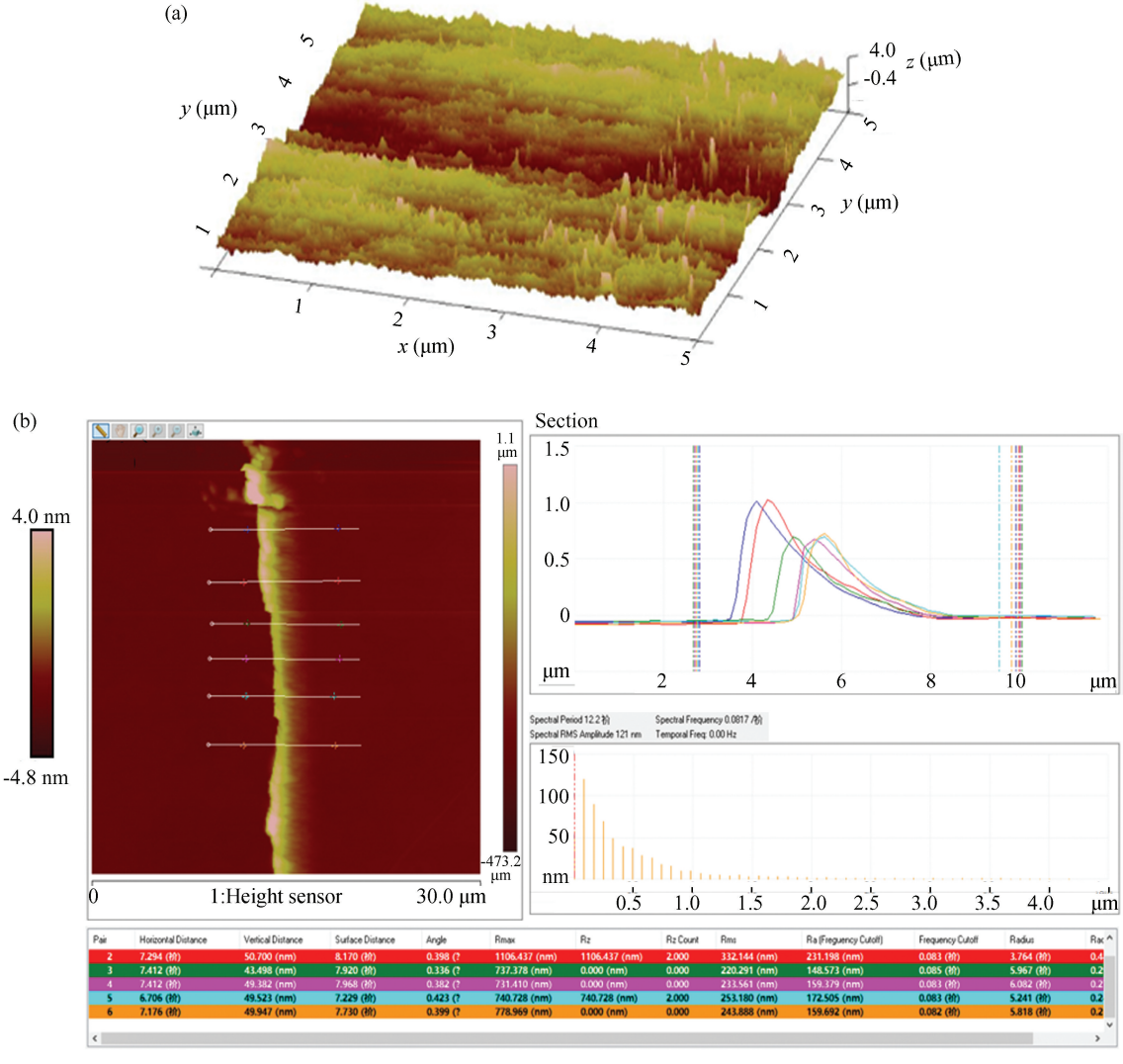


**Fig.2 (a) Step of thin film and (b) measurement diagram of film thickness**

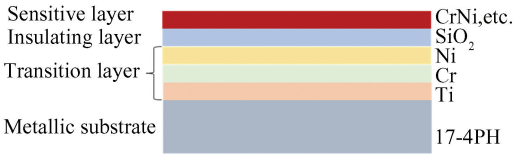


**Fig.3 Diagram of multilayer for metal-based MEMS sensor**

The thickness and matching of every single film are crucial to the properties of the transition multilayers. Then, the deposition process of the thin film is performed using the parameters as shown in Table 5. The influence of working pressure of argon gas and bias voltage is investigated by analyzing the surface roughness and thickness of film. At last, the bonding strength with the transition layer is evaluated by scratch tests using the Revetest Scratch Tester (CSM, Switzerland) and compared with that without the transition layer.

**Table 5 Deposition parameters of thin film**

| Degree of vacuum (Pa) | Sputtering power (W) | Argon flow rate (sccm) | Current of ion source(A) | Rotational speed (r/min) | Sputtering temperature | Time(min) |
|---|---|---|---|---|---|---|
| $5\times10^{-5}$ | 60 | 20 | 2 | 5 | Room temperature | 10 |

## 2 Results and Discussion

### 2.1 Effect of Working Pressure of Argon Gas

As the working pressure of argon gas increases from 0.3 Pa to 1.5 Pa, the sputtering rate gradually increases, and the thickness of film gradually increases, as shown in Fig. 4. The reason is that the higher the working pressure of argon gas, the more ionized gas it produces, and the more particles it bombards the target surface by the argon ions, which increases the sputtering rate[19].

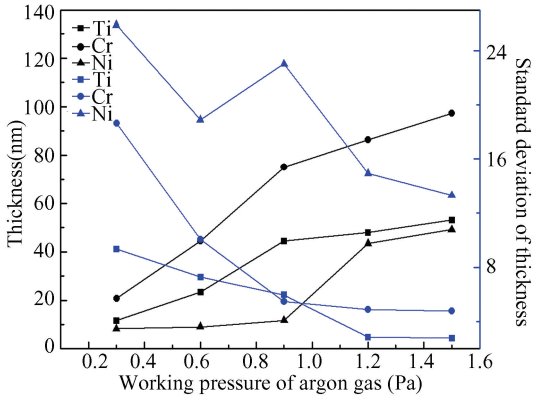


**Fig.4 Effect of working pressure of argon gas on the thickness of thin film**

For different materials, the sputtering rate is not the same. At the same parameters, the thickness of the Cr film is much bigger than that of Ti and Ni films. The reason may be differences in metallic bond energy. For example, they are 397, 470 and 428 kJ/mol for Cr, Ti and Ni elements, respectively. The small bond energy leads to the Cr atom being easily bombarded by argon ions, and tge thickness of the Cr film icreases.

At the same time, the standard deviation value of the film thickness gradually decreases, indicating that the uniformity of the film thickness is clearly improved. However, the standard deviation value of Ni film is much larger than that of Cr and Ti film, which may be induced by higher bonding energy and atomic mass.

The surface roughness of thin films is measured by AFM, and the average value is shown in Fig.5. For Ti and Cr films, the surface roughness *Ra* slightly decreases with the increasing of working pressure. Considering measurement error, the working pressure of argon gas has little effect on the average roughness of the thin film.

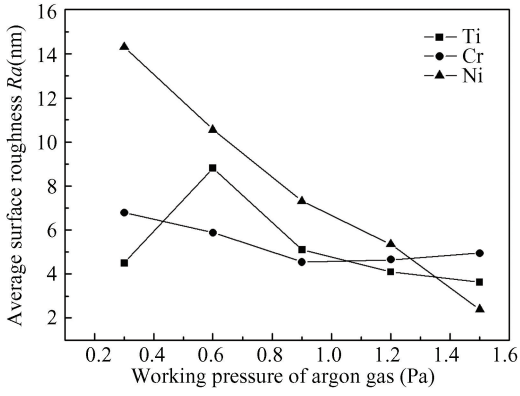


**Fig.5 Effect of working pressure of argon gas on the average surface roughness of thin film**

However, the surface roughness of Ni film decreases clearly with the increasing of working pressure of argon gas. For higher bonding energy and atomic mass, the sputtering rate is much lower, which leads to greater surface roughness. And, with the increasing of working pressure of argon gas, the

situation is changed since more Ni atoms are bombarded by argon ions. Then, a small surface roughness *Ra* is obtained for the Ni film at a higher argon gas working pressure.

## 2.2 Effect of Bias Voltage

Bias voltage gives more energy to the argon ions, and it has an obvious effect on the quality of thin film[20]. As shown in Fig. 6, the thickness of film gradually decreases with the increasing of bias voltage loaded on the substrate from 0 to 80 V. The reason may be that the bias voltage is too high, and the deposited atom may be bombarded and removed again by ionized gas with bigger energy, which can cause serious reverse sputtering, and reduce the sputtering rate. When the bias voltage increases within a certain range, the standard deviation of film thickness decreases, which means that the uniformity of thickness is improved. However, at a higher bias voltage, the standard deviation of film thickness increases again due to severe reverse sputtering, and its distribution of thickness becomes worse.

For different metallic elements, the thickness of the Cr film is the biggest one, and that of the Ni film is the smallest one. This can be attributed to differences in bonding energy and atomic mass among different elements.

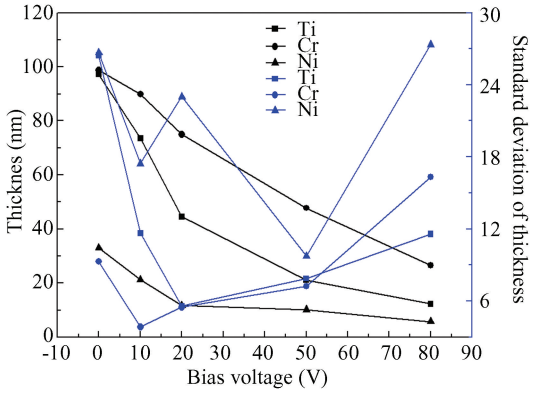


**Fig. 6 Effect of bias voltage on the thickness of thin film**

The surface roughness is shown in Fig. 7 for different bias voltages. And, the measurement results show that the average roughness changes a little for the Ti and Cr films, this indicates the bias voltage has a relatively small impact on surface roughness. However, the surface roughness of the Ni film increases clearly with increasing bias voltage. This may be attributed to severe reverse sputtering and a thinner Ni film.

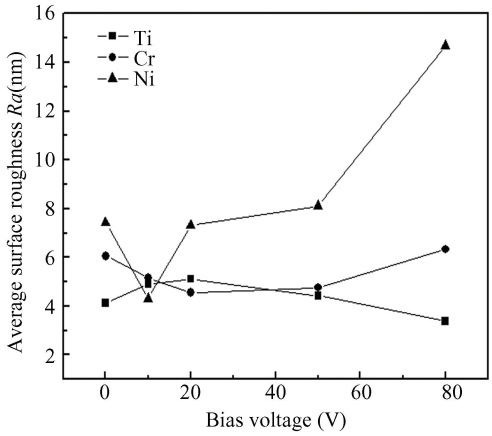


**Fig.7 Effect of bias voltage on the average surface roughness of thin film**

## 2.3 Determination of Sputtering Speed

Taking into account the sputtering rate and surface quality of thin film, working pressure and bias voltage are selected as 1.2 Pa and 20 V, 1.2 Pa and 10 V, 1.2 Pa and 10 V for the magnetron sputtering of Ti, Cr and Ni thin films, respectively, using argon gas in the flowing deposition of multilayer film. The influence of sputtering time on thickness is studied to obtain the accurate thickness of the designed film. Experimental results are shown in Fig. 8, and the obtained sputtering speeds are 4.07 nm/min, 8.19 nm/min and 4.27 nm/min for Ti, Cr and Ni thin films, respectively, which are important parameters for obtaining an accurate thickness of film during the deposition process of the transition multilayer film.

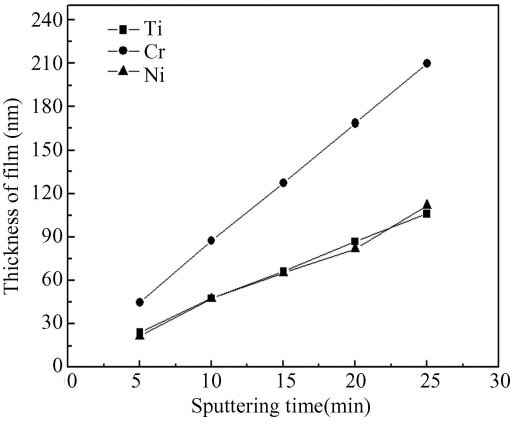


**Fig.8 Thickness of film under different sputtering time**

## 2.4 Deposition of Ti/Cr/Ni Multilayer

The deposition experiments are carried out using the parameters shown in Table 5 and Section 2.3. Different combinations film of materials and

thicknesses are designed as shown in Table 6. The thickness of each film can be obtained accurately by controlling the sputtering time based on the sputtering rate obtained by deposition experiments. In the test, the insulating layer is selected as the $SiO_2$ film prepared by the Plasma-Enhanced Chemical Vapor Deposition (PECVD) process.

**Table 6 Parameters of multilayer film**

| No. | Material | Thickness(nm) |
|---|---|---|
| 1 | Ti | 40 |
| 2 | Ti | 80 |
| 3 | Ti | 120 |
| 4 | Ti | 160 |
| 5 | Ti\Cr | 40\50 |
| 6 | Ti\Cr | 40\100 |
| 7 | Ti\Cr | 40\150 |
| 8 | Ti\Cr | 40\200 |
| 9 | Ti\Cr\Ni | 40\50\60 |
| 10 | Ti\Cr\Ni | 40\50\120 |
| 11 | Ti\Cr\Ni | 40\50\180 |
| 12 | Ti\Cr\Ni | 40\50\240 |

The adhesion strength between the metallic substrate and insulating layer is evaluated by scratch tests using the Revetest Scratch Tester (CSM, Switzerland) and compared with that without a transition layer. The diamond Indenter Rockwell AT-217 with an angle of 120° and an end radius of 200 μm is selected. The loading method is selected as linear step, the loading speed is set to 29.4 N/min, and the scratch length is 5 mm. Other parameters are shown in Table 7.

**Table 7 Parameters of scratch tests**

| Starting load(N) | Final load(N) | Moving speed (mm/min) | Acoustic emission sensitivity | Acoustic emission frequency(Hz) |
|---|---|---|---|---|
| 1 | 50 | 3 | 9 | 30 |

In the test, acoustic emission spectra, friction curves, and scratch morphology are used to comprehensively evaluate the critical load, and the critical load corresponding to this position is used to characterize the bonding force between adjacent layers. It is worth noting that some large particles, defects, and scratches deposited during the thin film preparation process can also cause sudden changes in friction signals and acoustic emission signals. At this time, it is necessary to distinguish abnormal peaks or inflection points by observing the scratch morphology to correct the critical load. From Fig.9, it can be seen that during linear loading, a semi-circular crack first occurs, followed by the accumulation and detachment of the film on both sides of the groove. And finally, the separation of the film from the substrate exposes the stainless-steel substrate.

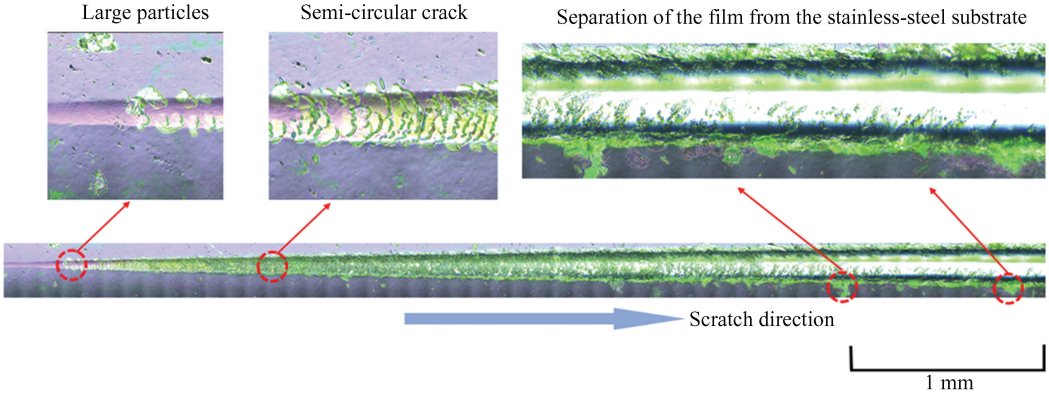


**Fig.9 Photograph of scratch**

The critical loads of all thirteen samples are shown in Table 8. Comparing samples from 1 to 4, only with Ti film as the transition layer material, when the thickness increases from 40 nm to 160 nm, the bonding force between the transition layer film and the stainless-steel substrate decreases from 28.77 N to 17.56 N, indicating that the bonding force of the single-layer transition layer film decreases with the increasing of the thickness. This may be because the material's compatibility deteriorates as the thickness increases, which leads to a gradual decrease in the membrane substrate bonding force. Meanwhile, compared with sample 13 without a transition layer, it can be seen that the Ti transition layer film can

effectively improve the film adhesion the metallic substrate. Compared to the bilayer and trilayer transition layers, the bonding force is lower.

With Cr and Ni films, comparing samples Nos.5–12 with samples Nos.1–4, it is found that the bonding strength of the Ti/Cr/Ni transition multilayer film is significantly improved, basically maintaining above 40 N. This means that the interfacial adhesion is improved, which is beneficial for the reliability of metal-based MEMS sensors. By analyzing samples Nos.5–8 and Nos.9–10, there is no clear pattern in the effect of thickness changes in Cr and Ni films on the bonding strength. However, compared to sample No.13 without a transition layer and samples Nos.1–4 with a single-layer transition layer, the bonding strength between the film and substrate is significantly improved, which can meet the requirements of metal-based MEMS sensors.

**Table 8 Bonding strength obtained by scratch test**

| No. | Materials and thickness(nm) | Critical load (N) |
|---|---|---|
| 1 | Ti-40 | 28.77 N |
| 2 | Ti-80 | 24.91 N |
| 3 | Ti-120 | 24.23 N |
| 4 | Ti-160 | 17.56 N |
| 5 | Ti\Cr-40\50 | 39.79 N |
| 6 | Ti\Cr-40\100 | 48.12 N |
| 7 | Ti\Cr-40\150 | 50 N+ |
| 8 | Ti\Cr-40\200 | 48.95 N |
| 9 | Ti\Cr\Ni-40\50\60 | 42.98 N |
| 10 | Ti\Cr\Ni-40\50\120 | 40.20 N |
| 11 | Ti\Cr\Ni-40\50\180 | 48.86 N |
| 12 | Ti\Cr\Ni-40\50\240 | 46.04 N |
| 13 | - | 15.11 N |

## 3 Conclusions

For metal-based MEMS sensors, a study was carried out on the preparation process of Ti, Cr, and Ni transition layer films on stainless-steel substrates, and the influence of hybrid transition layers was studied from the viewpoint of the bonding force between the substrate and the insulation layer using the scratch tests. Based on the experimental findings,

the following conclusions can be drawn:

1) As the working pressure of argon gas increases from 0.3 Pa to 1.5 Pa, the sputtering rate gradually increases for the more ionized gas. At the same parameters, the thickness of the Cr film is much larger than that of the Ti and Ni films, and the standard deviation value of the Ni film is much larger than that of the Cr and Ti films, which may be induced by higher bonding energy and different atomic mass.

2) The surface roughness *Ra* of the Ni film decreases clearly with the increase in working pressure of argon gas. However, it slightly decreases for the Ti and Cr films.

3) With the increase in bias voltage loaded on the substrate from 0 to 80 V, the thickness of the film and its standard deviation gradually decrease. The surface roughness of the Ni film increases clearly with increasing bias voltage, whereas it has little effect on the Ti and Cr films. This may be attributed to severe reverse sputtering and a thinner Ni film.

4) With Ti film as the transition layer, when the thickness increases from 40 to 160 nm, the bonding force between the transition layer film and the stainless-steel substrate decreases from 28.77 to 17.56 N, indicating that the bonding force of the single-layer transition layer film decreases with the increase in the film thickness.

5) It is found that the bonding strength of the Ti/Cr/Ni transition multilayer film is significantly improved, basically maintaining above 40 N. Compared to the sample without a transition layer or a single-layer Ti transition layer, the bonding strength between the insulating layer and metallic substrate is significantly promoted. This indicates improved interfacial adhesion, which is beneficial for the reliability of metal-based MEMS sensors under harsh working conditions.

## Conflict of Interest

The authors declare that they have no conflict of interest regarding the publication of this article.

## References


[1] Cao M Y, Laws S, Baena F R Y. Six-axis force/torque sensors for robotics applications: A review. IEEE Sensors Journal, 2021, 21 (24): 27238 - 27251. DOI: 10.1109/JSEN.2021.3123638.

[2] Xu J, Song A, Chen Y, et al. Research on a sixaxis force/torque sensor based on thin film sputtering technology and its decoupling for space robot. Measurement, 2025, 256(Part A): 117978. DOI: 10.1016/j.measurement.2025.117978.

[3] Wrbanek J D, Fralick G C. Thin film physical sensor instrumentation research and development at NASA Glenn research center. Cleveland: Glenn Research Center, 2006.

[4] Wrbanek J D, Fralick G C, Gonzalez J M, et al. Thin film ceramic strain sensor development for high temperature environments. Cleveland: Glenn Research Center, 2008.

[5] Liu H, Jiang S, Zhao X, et al. YSZ/$Al_2O_3$ multilayered film as insulating layer for high temperature thin film strain gauge prepared on Ni - based superalloy. Sensors and Actuators A, 2018, 279 : 272 - 277. DOI: 10.1016/j.sna.2018.06.032.

[6] Liu Y, Jiang H C, Zhao X H, et al. Microstructure evolution of thermally grown Al2O3 on NiCrAlY bonding coating for high-temperature thin-film sensors. Journal of Alloys and Compounds, 2022, 929: 167321. DOI: 10.1016/j.jallcom.2022.167321.

[7] Liu H, Mao X L, Jiang S W. Influence of substrate temperature on the microstructure of YSZ films and their application as the insulating layer of thin film sensors for harsh temperature environments. Ceramics International, 2022, 48(10): 13524 - 13530. DOI: 10.1016/j.ceramint.2022.01.231.

[8] Mengue P, Paulmier B, Hage-Ali S, et al. Temperature and strain SAW/BAW sensors on metallic substrates with RFID capability. Smart Materials and Structures, 2023, 32(9): 095017. DOI: 10.1088/1361-665X/aceaec.

[9] Wambach M, Ziolkowski P, Muller E, et al. Structural and functional properties of the thin film system Ti-Ni-Si. ACS Combinatorial Science 2019, 21(5): 362-369. DOI: 10.1021/acscombsci.8b00181.

[10] González G, Plogmeyer M, Schoop J, et al. Insitu characterization of tool temperatures using in-tool integrated thermoresistive thinfilm sensors. Production Engineering, 2023, 17: 319-328.DOI: 10.1007/s11740-023-01186-7.

[11] Feng Y F, Zhang Z, Qi R Z, et al. Microstructural evolution of Ni/Ti multilayers doped with nitrogen at different d-spacings for neutron supermirrors. Vacuum, 2023, 210: 111881.

[12] Zhang Q Y, Zhang Z, Ni H J, et al. Interfacial width and asymmetry evolution in Ni/Ti periodic multilayers with varying Ni thickness and neutron supermirrors with $m$ = 3. Thin Solid Films, 2025, 822: 140696. DOI: 10.1016/j.tsf.2025.140696.

[13] Guo Z R, Zhang Z, Huang Q S, et al. The effect of energy of Ar recoil particles on the interfaces and microstructure in Ni/Ti multilayer fabricated by direct current magnetron sputtering technique. Vacuum, 2024, 224: 113186. DOI: 10.1016/j.vacuum.2024.113186.

[14] Sakhonenkov S S, Gaisin A U, Konashuk A S, et al.

Influence of silicon interlayers on transition layer formation in Ti/Ni multilayer structures of different thicknesses. Journal of Physics and Chemistry of Solids, 2025, 207:113003.DOI:10.1016/j.jpcs.2025.113003.

[15] Zhao S N, Zhu J T, Yang Z H, et al. Interface and crystallization evolution induced by reactive nitrogen and oxygen sputtering in Ni/Ti multilayer. Surface & Coatings Technology, 2023, 472: 129941. DOI: 10. 1016/j. surfcoat.2023.129941.

[16] Frankel D J, Moulzolf S C, Pereira da Cunha M, et al. Influence of composition and multilayer architecture on electrical conductivity of high temperature Pt-alloy films. Surface & Coatings Technology, 2015, 284: 215-221. DOI:10.1016/j.surfcoat.2015.08.074.

[17] Pei S B, Yang F F, Feng N X, et al. On the thermal stability and oxidation resistance of $Zr/X_{(Cr, Ni, Si)}$ multilayer structure. Surface & Coatings Technology, 2022, 440: 128500. DOI: 10. 1016/j. surfcoat. 2022. 128500.

[18] Ren Z Q, Wu W G, Song D, et al. The effect of annealing process on the performance of strain nickel-chromium thin film sensor. AIP Advances, 2020, 10: 105030. DOI:10.1063/5.0026353.

[19] Khalaf M K, Al-Alwany R M S, Salman I K. Effect of working pressure on the structural and morphological properties of gold nanoparticles prepared by a dc magnetron sputtering technique. Journal of Critical Reviews,2020,7(1):171-175.

[20] Vassallo E, Pedroni M, Saleh M, et al. Effect of negative substrate bias voltage and pressure on the structure and properties of tungsten films deposited by magnetron sputtering technique. Coatings, 2025, 15(3): 319.DOI:10.3390/coatings15030319.